Transient current and sheath motion following the photoelectron-initiated avalanche in dc glow discharges

H. Debontride, J. Derouard, P. Edel, R. Romestain, and N. Sadeghi
Laboratoire de Spectrométrie Physique, Université Joseph Fourier–Grenoble 1, Boîte Postale No. 87, 38402 Saint-Martin-d'Heres CEDEX, France

J. P. Boeuf
Centre de Physique Atomique de Toulouse, Université Paul Sabatier, 118, route de Narbonne, 31062 Toulouse CEDEX, France
(Received 21 April 1989)

We have performed time-resolved observations of the current, optical emission, and electric field profiles in an Ar +2% K dc glow discharge, following the pulsed-laser-induced photoelectron emission on the cathode. These observations indicate that (1) The photoelectron-initiated avalanche results in a strong perturbation of the charge distribution in the discharge. This can be observed as a considerable shortening of the sheath length. (2) This leaves the discharge in a nonstationary regime, with a highly enhanced conductance. It then relaxes to the initial, steady-state regime in a time which is about 100 μs in our conditions. This time is both considerably larger than the ion transit time in the sheath and shorter than the ambipolar diffusion time. Self-consistent macroscopic simulations have been done and found to be in excellent qualitative agreement with the observations. Monte Carlo microscopic simulations of the ionization in the sheath have also been performed to point out some shortcomings of the "beam model" used in the self-consistent simulations.

I. INTRODUCTION

In this paper we present some observations and numerical simulations, yet preliminary, concerning the motion of the sheath following the sudden release of a bunch of electrons at the cathode of a dc discharge. This is induced by the photoemission resulting from the impact of a pulsed-laser beam on the cathode.

As shown previously,[1-3] the avalanche that develops in the discharge yields a considerable increase of the current, which constitutes what is known[1] as the photoemission optogalvanic (POG) signal. The POG effect has been recently demonstrated[1,2] to be a potentially interesting phenomenon for the *in situ* diagnostic of surfaces in etching reactors. Beside this, its understanding is strongly related to that of rf and other nonstationary discharges: In some respects the POG effect is the response of the discharge to an almost instantaneous perturbation, and its observation yields directly the relevant characteristic time scales. In addition, the analysis of the time dependence of the observed POG signals may give some information about the secondary-electron-emission coefficient by ion impact on the cathode, by analogy with the methods used by Varney[4] a long time ago in non-self-sustained discharges.

Previous investigations[1-3] on the POG effect have focused on the short-time scale (≤ 100 ns) on which the electron avalanche develops in the gas. In the present work more attention has been paid to the study of larger time scale phenomena 100 ns $\leq \Delta t \leq 100$ μs where heavy particles are involved.

Spatially and temporally resolved spectroscopic diagnostics have allowed us to probe the variation of the electric field, then the motion of the sheath and the dramatic space-charge modifications which result from the POG effect. In addition, self-consistent macroscopic and Monte Carlo microscopic calculations have been performed. Many of the experimental observations can be qualitatively reproduced by the self-consistent model. Analysis of the Monte Carlo simulations of the ionization in the sheath is very informative and shows the way for a better, *quantitative* description of the phenomena.

Compared to the work reported by Mitchell, Scheller, Gottscho, and Graves,[3] our experimental conditions differ by several points: first, by the magnitude of the ratio of the POG current to the steady-state current which is of several hundreds in our case. Indeed our steady-state current densities are much smaller than Mitchell *et al.*[3] due to smaller applied voltages and smaller gas densities; second, by the pulse duration of the photoemission laser source (a copper vapor laser), which is several tens of ns, much longer then the time scale on which the avalanche develops in the sheath; third, by the nature of the gas used in our discharge, which is a mixing of Ar (98%) and K(2%). This mixture has been chosen because it allows the space- and time-resolved diagnostic of the electric field[5-7] using NaK molecules,[8-10] present as traces in such alkali-metal vapors, as a spectroscopic probe; the alkali-metal vapor affects the ionization processes; it also affects the surface of the cathode, on which it is likely that an alkali-metal layer is formed, and thus the secondary-electron-emission coefficients and the photoelectron yield are affected, too; fourth, let us emphasize that our experimental conditions are restricted to what is

called by Mitchell *et al.*[3] the "low-power regime": Our applied voltage is at most 254 V while theirs is at least 250 V, up to 350 V. Our conclusions about the description of the phenomena are basically the same as Mitchell *et al.*[3]

II. EXPERIMENT

A. Principle

A pulsed-laser beam is sent onto the cathode of a dc discharge established in a mixture of Ar and alkali-metal vapor (mostly K atoms). The photoelectrons which result initiate an avalanche in the plasma. We monitor the corresponding transient current and the space- and time-resolved electric field and plasma-induced optical emission. The electric field amplitude is determined using the Stark effect observed in the laser-induced fluorescence spectrum of NaK molecules,[5-10] present as traces in the gas of the discharge. Let us describe now the different parts of the experimental setup shown on Fig. 1.

B. Discharge cell

The discharge is established in a cylindrical Pyrex cell (external diameter 6 cm) with two parallel 3-cm-diam stainless-steel electrodes. The separation between the electrodes is 3.5 cm. Their reverse side is covered with a Pyrex cap to avoid the formation of a discharge in the volume outside the volume which faces both electrodes. One electrode is held 50 Ω above ground while the other is connected to a dc voltage supply through a 43-kΩ load. A 1-μF capacitor connected to the ground ensures that the voltage between the electrodes remains constant during the characteristic time of the transient current ($\sim$ 100 μs). The voltage across the 50 Ω serves to probe the discharge current. It is monitored using a boxcar integrator (SRS Model 255) interfaced to a PC computer and triggered by the signal of a fast photodiode irradiated by a reflected beam of the photoemission laser. The signal to monitor is properly delayed using a 500-ns delay line.

The cell is located inside an oven where a temperature of 210 °C is controlled using a thermocouple and stabilized within 1 °C. It is connected to a vacuum system which allows it to evacuate and fill with Ar gas. It contains also a small amount of K and Na in the molar fraction 2:1, respectively.

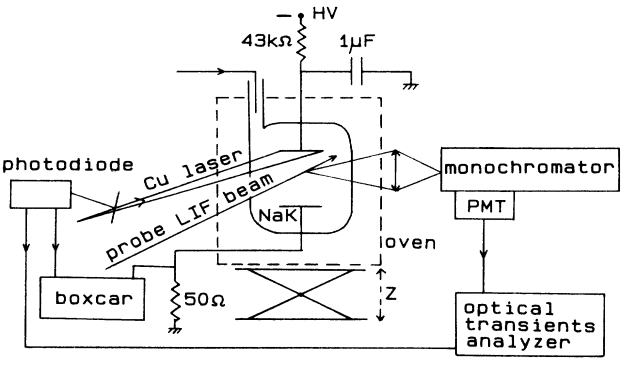

FIG. 1. Experimental setup.

The composition of the alkali-metal vapor in the cell can be estimated from known thermodynamic data[10] to be about 1.5×10^{14} K atoms/cm^3, 3.07×10^{12} Na atoms/cm^3, 2.30×10^{11} K_2 molecules/cm^3, 6.61×10^{10} NaK molecules/cm^3, and 4.47×10^{9} Na_2 molecules/cm^3 at 210 °C. The gas of the discharge can thus be considered as a mixture of mostly Ar, and a small fraction of K atoms. In the present experiment, the total pressure in the cell was 0.4 Torr corresponding thus to 78.5×10^{14} Ar atoms/cm^3+2% K atoms. The pressure is monitored using a MKS capacitance manometer. It does not change by more than 10 mT during the course of an experiment.

C. Photoemission source

A pulsed Cu vapor laser (Oxford Lasers model CU 60) is used as the photoemission light source. Two lines are emitted (510.5 and 578.1 nm) with approximately the same intensity, at a repetition rate of 6.50 kHz. We have recorded the time profile of these pulsed emissions, and found roughly the same shape for the green and yellow lines. The pulse shape of the green emission can be seen on Fig. 2. Note the relatively large duration of the emission about 30 ns FWHM, 65 ns total time.

The laser beam is properly attenuated, collimated, and directed onto the surface of the cathode with an angle of incidence of approximately 60°. It is expanded to completely cover the electrode surface. We estimate the incident energy on the whole cathode to be about 3(μJ/pulse)cm^{-2} taking into account the expansion of the beam, and the transmittance through the windows of the oven and the cell. This estimate is approximate and only its order of magnitude is significant.

It may seem astonishing that photoemission occurs on

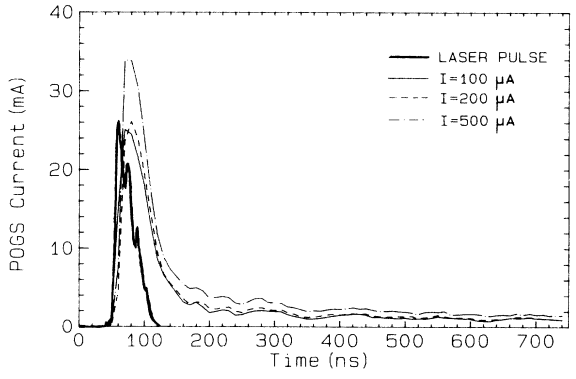

FIG. 2. Photemission optogalvanic signals and pulse shape of the Cu laser green emission (510.5 nm) shed onto the cathode (the yellow emission has roughly the same shape), as a function of time for three different discharge currents. Discharge conditions are Ar 98%, K 2%, 0.4 Torr 210 °C, $I_0=100$ μA (14 μA/cm^2), 200 μA (28 μA/cm^2), 500 μA (70 μA/cm^2). The integrating gate width is 10 ns.

stainless steel, whose work function is about 4.5 V,[11] when illuminated with photons whose energy is only 2.43 eV (510 nm) or 2.15 eV (578 nm). This, in fact, is the proof that the surface of the cathode is strongly affected by the alkali-metal vapor which is likely to form a layer on it. Note that the work function of K and Na are 2.3 and 2.75 eV, respectively.[12] Let us mention that we have checked that no photogalvanic signal can be detected when the laser lights the gas in the cell without hitting the cathode: The photoemission occurs only on the surface of the cathode, not in the volume of the gas. We have observed that the photogalvanic current, hence the photoemission yield significantly changes from day to day, but is fairly constant during the course of an experiment.

D. Optical diagnostics

The optical emission from the cell is imaged onto the entrance slit of a 2-m monochromator and detected by a photon counting system. The oven plus cell setup is mounted on a jack to allow the determination of spatial profiles.

For plasma-induced emission observation the spatial resolution is about 1.5 mm along the axis of the discharge taking into account the aperture of the optics and the fact that the emission is spread over the whole diameter (3 cm of the cathode). For laser-induced fluorescence observation, this spatial resolution reduces to 0.7 mm taking into account the slit width of the monochromator (0.3 mm) and the spatial extension of the laser beam (whose profile after expansion by a cylindrical telescope is a rectangle 10×1 mm^2; such an expansion is done to reduce optical pumping effects[13] while keeping a good fluorescence intensity level).

The laser-induced fluorescence of NaK molecules is used to determine the space- and time-resolved electric field through the *e-f* Stark mixing effect.[5–10] We use for this a single-mode dye laser tuned to the proper NaK ($X\,^1\Sigma^+ - B\,^1\Pi$) transition.[8–10] The electric field is deduced from the Q to R fluorescence lines ratio, using calibration curves established previously[7] from spectroscopic data.[10]

E. Optical signals transient analyzer

Both plasma-induced and laser-induced signals are recorded on a homemade fast transient analyzer triggered by the photodiode signal induced by the photoemission source laser pulse. Here follows a brief description of this transient analyzer, a detailed diagram of which will be published elsewhere.

It consists of 64 independent high-speed 100-MHz counters. Each channel can count up to 2^{26} pulses. The photon pulse is switched to the counter corresponding to its arrival time by a system using a shift register operated by a clock, the period of which is a multiple of the mean clock. The mean clock runs at 80 MHz and is synchronized at the beginning of each run (i.e., at each laser pulse); this avoids any jitter between the clock and the start pulse. The time width of each channel is thus a multiple of 12.5 ns. The main difficulty in such an apparatus is that this time width should be independent of the channel. This difficulty has been bypassed by obtaining counting pulses synchronous of the mean clock and arriving neither at the opening nor at the closing of any channel despite the random arrival of the photon pulses. The dead time during a run is low enough to ensure that 80% of the events are effectively taken into account. As the memory corresponding to each channel is actually a counter there is no dead time at the end of each run, due to transfer or computing. The repetition rate can thus be larger than 1 MHz.

III. EXPERIMENTAL RESULTS

A. Photo-optogalvanic current

Figures 2 and 3 show the time dependence of the transient current which follows the photoelectron emission for different steady-state discharge currents. Figure 2 shows the short-time scale, together with the laser-induced photoemission, indicated by the laser pulse shape. We observe the very intense POG signal: Its magnitude is in our conditions more than hundreds of times the value of the steady-state current of the discharge. The POG signal is synchronized with the photoemission laser pulse, but continues to increase after the maximum of the photoemission is reached. Moreover, we have found that it is, to a large extent, proportional to the photoemission laser intensity, although it tends to saturate for laser fluxes larger than 30 μJ/pulse cm^2 (which is an order of magnitude larger than the present conditions), probably because of space-charge effects, as shown previously by Downey *et al.*[1]

We see that in our conditions the POG intensity does not seem to depend very much on the discharge power, contrary to observations by Mitchell *et al.*[3]; we will come back to this point later in the discussion (end of Sec. IV D). But let us recall that our measurements are restricted to the "low-power" regime, where actually

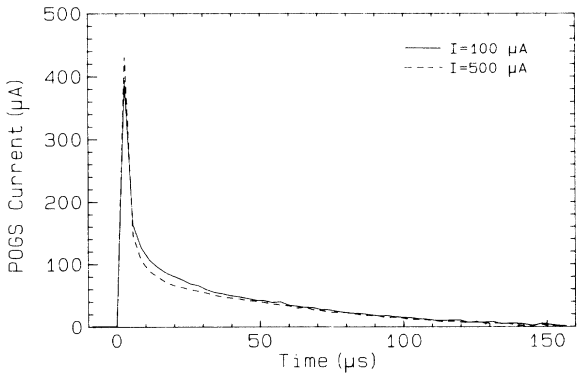

FIG. 3. Photoemission optogalvanic signals as a function of time. Same conditions as Fig. 2. The integrating gate width is 3 μs. The steady-state current has been subtracted off. Note that the current has reached its steady-state limit (POG current = 0) before the arrival of the next photoemission laser pulse.

Mitchell *et al.* found little power dependence.

After the fast-electron avalanche which results from the photoemission, the plasma is left with strongly perturbed ion and electron densities. It then relaxes back to the steady-state regime. This is what Fig. 3 shows with the long-time scale dependence of the discharge current. We see that it takes about 100 μs for the plasma to recover its steady-state current, before the arrival of the next photoemission laser pulse. We also observe a noticeable dependence of the decreasing of the current at medium time scale 7–30 μs with the discharge power.

Although much smaller than the POG signal observed during the photoemission avalanche, this long-time scale current is still considerably larger than the steady-state current. Its time integration yields an "optogalvanic charge" which is about 6–7 times the integration of the optogalvanic current during the photoemission.

Finally let us mention that we have found that in our conditions (Ar, 98%; K, 2%, 0.4 Torr, 210 °C), the time-averaged optogalvanic current (integrated over the time interval between two photoemission pulses) does not change by more than 10% when the discharge current density varies between 1 and 30 times the normal regime value. This result does not seem to persist for higher pressures, however, and may be fortuitous.

B. Plasma optical emission

Not surprisingly, the current increase which follows the photoemission is accompanied by a considerable increase of the optical emission of the plasma. The time dependence of this emission comprises again a short-time scale, which corresponds to the excitation by the beam resulting from the photoemission on the cathode, and a long-time scale which corresponds to the relaxation of the discharge.

Similarly to Mitchell *et al.*,[3] we have found that the short-time dependence of the emission does not depend on the position inside the discharge (although its magnitude does) which is consistent with the beam excitation. However, the long-time scale (Fig. 4) shows that the emission does not behave everywhere the same.

Note that the optical emission has not completely recovered its steady-state level 150 μs after the photoemission. Perhaps this is associated with the fact that K atoms may be excited by collisions involving long-lived Ar metastable states. Very interesting insights about the discharge behavior are provided by the time-resolved spatial emission profiles. The results are shown on Figs. 5 and 6 together with the electric field profiles which we are now going to present.

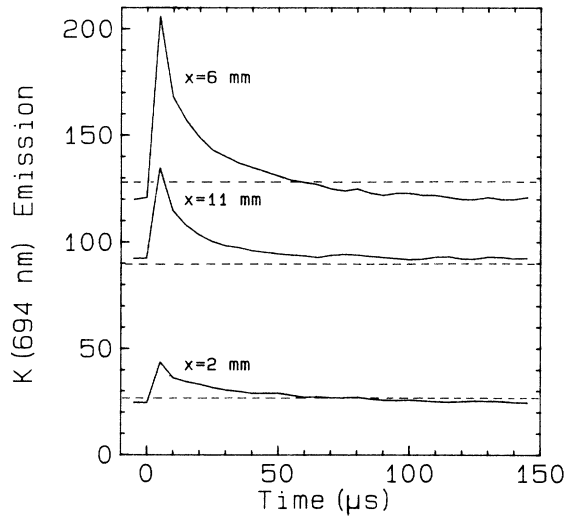

FIG. 4. K atom emission at 693.3 nm ($6s\ ^2S_{1/2}-4p\ ^2P^0_{1/2}$ transition) as a function of time for three different positions in the discharge. Same discharge conditions as Fig. 3, 500 μA, steady-state sheath length 6 mm. Integration gate width is 5 ns. Note that the emission has not completely reached its steady-state level 150 μs after the photoemission pulse, and that the emission intensity may be larger or smaller than the steady-state level, depending on the position. This may be the indication of excitation processes via long-lived metastable states.

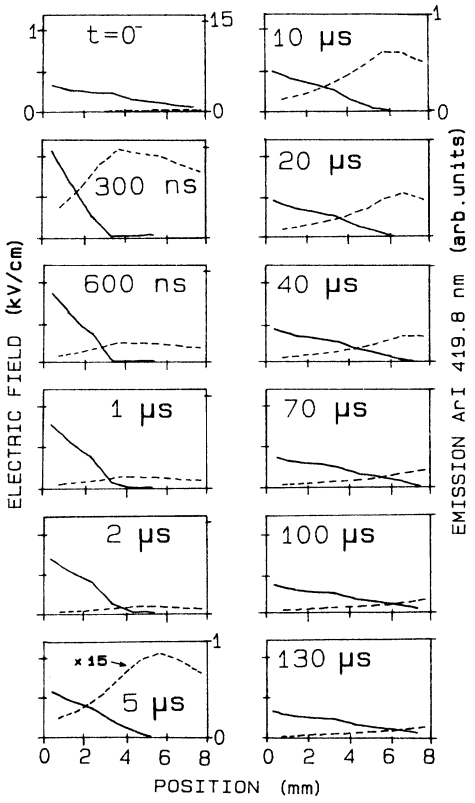

FIG. 5. Amplitude of the electric field (continuous line) and Ar atom emission at 419.8 nm ($5p[\frac{1}{2}]_0-4s[1/2]^0_1$ transition) profiles as a function of time. Discharge conditions are 100 μA (14 μA/cm^2), V=154 V, Ar(98%)+K(2%), 0.4 Torr, 210 °C. These conditions correspond to the POG signal shown in Figs. 2 and 3. Note the change in the scale of the Ar emission signal at $t=5$ μs.

C. Sheath electric field measurements

On Figs. 5 and 6 are shown the dependence of the electric field profile with time, determined using the time-resolved Stark *e-f* mixing spectroscopy of NaK (Refs. 8–10) described above. On the same time scale are shown the optical emission profiles of the Ar atom $\lambda = 419.8$ nm, $5p[\frac{1}{2}]_0$-$4s[\frac{1}{2}]^0_1$, transition. Time is indexed with respect to the arrival of the photoemission pulse, which is repeated every 150 μs.

Just before the arrival of the photoemission pulse (time labeled "0") the shapes of the electric field profile closely reproduce the steady-state cases.[9] The sheath edge is marked both by the maximum of the optical emission and by the vanishing of the electric field, as usual.

But just after the photoemission and the associated avalanche, one sees the dramatic shortening of the sheath and the increase of the field at the cathode. (The voltage is maintained constant so that one expects the area under the field profile to remain constant.) This increase of the field is associated with a large displacement current $\epsilon_0(\partial E/\partial t)$ which is an important contribution to the POG signal at the short-time scale.

Correlatively, note the considerably enchanced optical emission, and the shift of the maximum in the spatial profile toward the cathode. Afterwards one observes the motion of the sheath which eventually recovers its initial shape between 100 and 150 μs. Note that at each time, the emission intensity profile monitors the sheath length, as one expects.[14,15]

We have observed that the sheath edge propagates with a velocity which is independent of the discharge power while $t < 5$ μs. Then it slows down for the higher power but continues to expand for the lower power, as the final sheath length is longer in the latter case. This difference in the sheath edge propagations may be correlated with the splitting between the POG curves observed for $5 < t < 30$ μs (see Fig. 3).

Note also the dependence of the general shape of the field profiles to the discharge power. While the field profile remains close to a straight decreasing line for $I_0 = 100$ μA, it clearly shows a curvature for $I_0 = 500$ μA: This indicates that the space charge is not uniform in this latter case, but increases from the cathode to the sheath edge, a phenomenon already seen in (Refs. 16 and 17) and (Ref. 6) discharges.

Finally let us mention that we have checked that the integral of our electric field profiles over the sheath length gives the applied voltage generally within 10%. This is consistent with the fact that no detectable electric field (i.e., larger than 30 V/cm) could be seen outside the cathodic region.

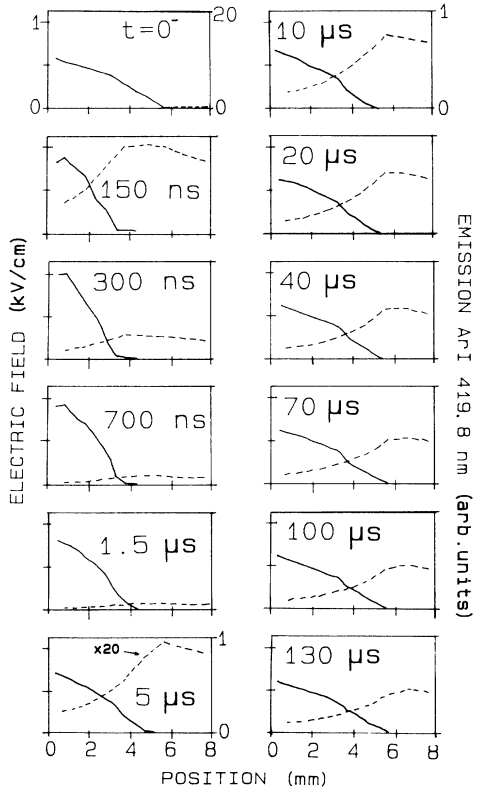

FIG. 6. Same as Fig. 5 with $I_0 = 500$ mA (70 mA/cm^2), $V = 224$ V.

IV. NUMERICAL SIMULATION

In order to improve our physical understanding of the phenomena described above, we have performed numerical simulations of the POG effect in our experimental conditions.

A. Self-consistent beam model

The ideal way of modeling a glow discharge (and especially the cathode region of a glow discharge) would be to solve the electron and ion Boltzmann equations coupled with Poisson's equation. This is still a difficult numerical problem, and a simpler approach is necessary. Our approach is based on the description of electron and ion transport by moments of the Boltzmann equation. The main difficulty in this approach is to obtain a realistic description of the ionization rate in the cathode region (cathode fall and negative glow), knowing that in this region there is no equilibrium between electron kinetics and local electric field. Since the parameters (mean energy, velocity) characterizing the electrons emitted by the cathode and accelerated through the sheath are very different from those of the plasma bulk electrons of the negative glow, we have chosen to consider two different groups of electrons, their kinetic properties being defined as follows.

(i) Fast electrons (or beam electrons) accelerate in the sheath and lose their energy in the glow through inelastic collisions; these electrons are assumed to form a monoenergetic beam[18] whose velocity is directed toward the anode. Secondary electrons created by ionization by the fast electrons are assumed to belong to the beam if they are created in the sheath; when the ionization takes place in the glow, the secondary electrons join the low-energy group which is described below. The transport of the fast

electrons is described by a continuity equation and an energy equation. The beam is supposed to release instantaneously its energy in the discharge (the continuity and energy equations for the beam are steady-state equations). This approximation has some consequences and leads to errors on the short-time scale (of the order of 10 ns in our conditions) but for larger time scales, we think that it is realistic enough for our purpose.

(ii) Low-energy electrons (bulk electrons) are created in the glow by ionization due to fast electrons; when the beam energy falls below the ionization threshold, fast electrons join the low-energy group. The kinetics of the low-energy group is described by a continuity equation and a momentum-transfer equation.[19] The momentum-transfer equation for the bulk electrons (as well as for the ions) is simplified by omitting the time derivative term and neglecting the drift energy with respect to the thermal energy, such as in Ref. 19; this neglect of the inertia terms is reasonable in a collisional regime and leads to the representation of the particle flux by the sum of a drift term and a diffusion term.

The boundary conditions are as follows: the gap voltage is given and constant, the density of bulk electrons and ions on the electrodes is zero, and the flux of beam electrons leaving the cathode is proportional to the flux of ions reaching the cathode (coefficient γ). Note that the basic data needed by the model are the transport coefficients for bulk electrons and ions (drift velocity and diffusion coefficient), and the electron-atom cross sections for the beam electrons.

The equations describing the two electron groups, and the ion continuity and momentum-transfer equations are coupled to Poisson's equation. The model can provide the spatial and temporal variations of the electric field, charged particle densities, and current densities in the different regions of the discharge for a given applied potential. A more complete description of the model can be found in Refs. 20 and 21.

In order to simulate our experiment, we first model a steady-state dc discharge corresponding to the experimental conditions just before the laser pulse; the discharge is in that case self-sustained by the ion bombardment on the cathode, which releases secondary electrons; the relation between the flux of electrons emitted by the cathode and the flux of ions toward the cathode (which defines the secondary-electron-emission coefficient) is a boundary condition of the model. The action of the laser pulse on the cathode is then represented in the model by a given flux of photoemitted electrons which is added to the flux of secondary electrons.

Due to the simplifying assumptions used to describe the beam electrons (see above), this model is, however, not adequate for the case of a gas mixture containing species of very different ionization potentials such as Ar and K. We have just neglected, in a first step, the influence of the 2% K atoms. The validity of this assumption will be considered below where we present Monte Carlo simulations of the ionization in the sheath, in the actual 98% Ar, 2% K mixture.

We give below a few facts concerning the numerical method: (a) the method is based on a finite-difference representation of the transport equations and Poisson's equation; the discretization scheme of the electron and ion continuity equations is similar to the Gummel scheme described in Ref. 19. (b) Contrary to Ref. 19 the transport equations and Poisson's equations are solved in an implicit way and not successively; the equations are first linearized with respect to the three variables (electron density, ion density, electric potential): This leads to a bloc-tridiagonal system which is easily solved by standard methods. Since larger time steps can be used, this implicit method is much faster than the one described in Ref. 19. (c) The principles and details of the numerical method can be found in Ref. 22.

B. Modeling procedure

The modeling procedure is as follows: First we begin by trying to reproduce the steady-state discharge: Given a discharge voltage V, we adjust the secondary-emission coefficient by ion impact on the cathode γ so that the result of the self-consistent simulation yields a sheath length equal to the one experimentally found. Assuming that the secondary-emission coefficient is constant for different discharge voltages we check that the same value of γ gives a correct estimation of the sheath length for other values of the applied voltage. Since we have been working in a range of discharge voltages limited to 154–224 v the assumption of a constant γ seems reasonable. The consistency (if not the validity) of the procedure can then be inferred by checking that the calculated discharge current in these conditions roughly agrees with the experiment.

In the present case, two experimental conditions have been considered.

Case 1. $J_0=14$ μA/cm^2 ($I_0=100$ μA); V=154 V, $d_c=10$ mm (d_c is the sheath length).

Case 2. $J_0=70$ μA/cm^2 ($I_0=500$ μA); V=224 V, $d_c=6$ mm, which correspond to Figs. 5 and 6, respectively. No external circuit is considered, and the potential between the electrodes is supposed to be constant during the experiment (see above).

The calculations are performed for the case of pure argon, and the Ar pressure is chosen equal to 0.25 Torr at 300 K, corresponding to the experimental conditions of 0.4 Torr at 210 °C. The mobilities of the bulk electrons and ions in pure argon are taken from Ward;[23] their diffusion coefficients are supposed to be constant (3×10^5 and 2×10^2 cm^2/s, respectively, for electrons and ions at 1 Torr, 300 K). The electron-atom inelastic cross sections which are used in the beam equations are taken from Bretagne *et al.*[24] The gap length is 35 mm; the model is monodimensional and ignores the radial effects associated with the finite diameter (30 mm) of the electrodes.

It turns out that a value of $\gamma=0.07$ yields the sheath lengths observed experimentally in both cases, giving current densities of 8 and 55 μA/cm^2 in cases 1 and 2, respectively, in fair agreement with the experiment. Then the photoemission process is modeled by imposing an additional electronic current at the cathode. Starting from steady-state conditions, the evolution of the system is fol-

lowed step by step. The model yields the time dependence of the electric field, electronic and ionic density profiles, and current densities.

In the present calculations, the photocurrent has been chosen equal to 500 $\mu A/cm^2$ during 50 ns. While 50 ns corresponds roughly to the duration of the photoemission laser pulse (see Fig. 2), the value of 500 $\mu A/cm^2$ is rather arbitrary, because it is difficult to estimate experimentally. This value of the photoemission current should be adjusted such that the predicted discharge current matches the observed POG amplitude (Fig. 2). Results of the calculations seem to indicate that the photocurrent may be larger than 500 $\mu A/cm^2$; simulations for larger photocurrents lead to numerical instabilities.

C. Results and discussion

Figure 7 shows the spatial variations of the electric field and charged particle densities for the unperturbed steady-state dc discharge corresponding to cases 1 and 2. The transient results, showing the time evolution of the field and charged particle density profiles in the discharge during and after the laser pulse are presented in Figs. 8 and 9. The time variations of the current densities are plotted in Fig. 10.

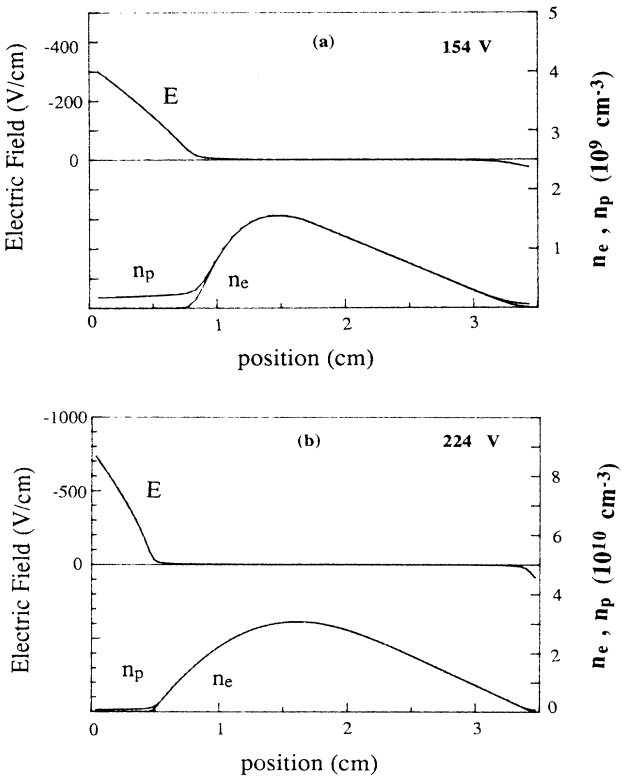

FIG. 7. Spatial variations of the electric field and charge particle density profiles for the unperturbed steady-state dc discharge obtained with the self-consistent model. (a) 8 $\mu A/cm^2$, 154 V and (b) 55 $\mu A/cm^2$, 224 V. Note the negative scale of the electric field vertical axis: A positive electric field would point outward from the cathode.

Let us note first an important feature of the unperturbed steady-state dc discharge which appears in Fig. 7 (and also in Figs. 8 and 9): There is a field reversal in the negative glow. This field reversal is due to the fact that the beam electrons act as an external ("nonlocal") ionization source in the glow. In the glow and close to the anode, the two components of the electron flux (drift term and diffusion term) have opposite directions and their amplitude is much larger than the amplitude of the total electron flux. The field tends to maintain the electrons in the plasma while they can reach the anode by a diffusion process. The plasma potential is therefore positive with respect to the anode potential and is linked to the electron energy in the glow. These features have been suggested empirically[25] for a long time but it is only very recently that numerical self-consistent models have been able to predict them[20,21,26] and that experiments proved their existence with no ambiguity[27] as discussed in a recent paper by Gottscho *et al.*[27] Note that this field reversal does not occur when an equilibrium model is used (a model where the ionization rate is supposed to depend only on the local electric field) and is related to the fact that the beam electrons act as an external ionization source in the glow.[20,21,28]

Let us now consider (Figs. 8 and 9) the transient behavior of the field and charged particle densities in the discharge, after the onset of the photoemission current ($t = 10$ ns). The predicted spatio-temporal variations of the electric field are very similar to those observed experimentally, although the quantitative agreement is not as good for case 2 (corresponding to the larger steady-state discharge current: 55 $\mu A/cm^2$). Figures 8 and 9 show very interesting features, which we are now going to discuss.

We see that as soon as the photocurrent is switched on, an enhanced ionization occurs in the plasma, which results in the following.

(i) The enchancement of the charge densities both in the sheath and in the glow. Note that as can be expected the relative perturbation of the plasma density seems to be much more important in case 1 than in case 2; this is due to the fact the predicted plasma density in the steady-state unperturbed dc discharge corresponding to case 1 is much smaller than in the discharge corresponding to case 2 (see Fig. 7).

(ii) The contraction of the sheath and, correlatively, the increase of the sheath electric field; these effects are induced by the fact that the ion density increases in the sheath and that the potential across the discharge is constant.

(iii) The enhancement of the current (POG). The total current at any point of the discharge is the sum of the displacement current and the electron and ion conduction currents; Figs. 8 and 9 can be used to obtain a very simple estimation of the displacement current ($\epsilon_0 \partial E/\partial t$) on the cathode; it turns out that on the cathode, the displacement current is of the same order as the photoelectron current [Figs. 10(a) and 10(b)] (which has been supposed to be 500 $\mu A/cm^2$ in the calculations); the contri-

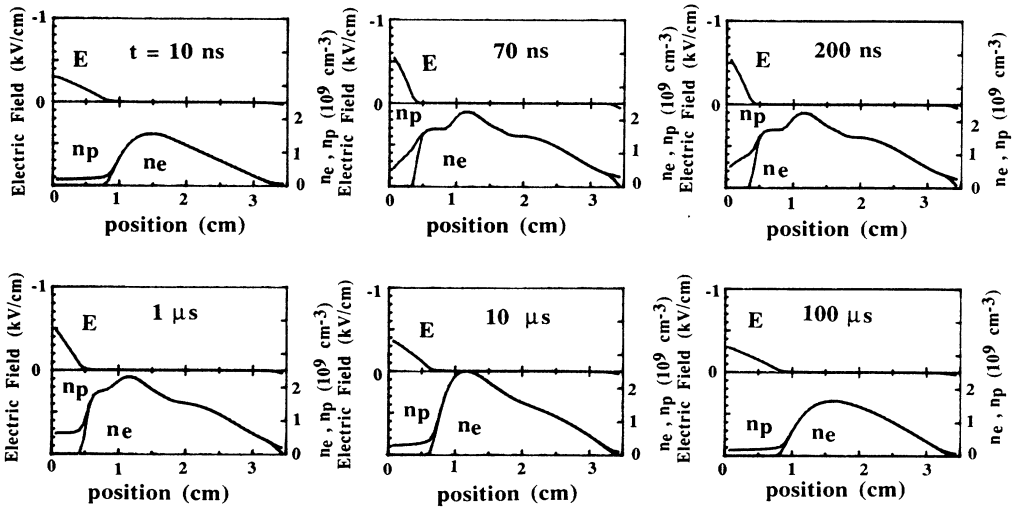

FIG. 8. Electric field and charged particle density profiles as a function of position, at different times, as predicted by the numerical self-consistent macroscopic model. Discharge conditions corresponding roughly to Fig. 5 (8 μA/cm^2, 154 V, but pure Ar, 0.25 Torr at 300 K). The photoemission has been simulated by imposing a constant electron current of 500 μA/cm^2 during the time interval 10 ns $< t <$ 60 ns.

bution of the ion current to the total current on the cathode is negligible during the laser pulse. On the anode, the dominant component of the total current is the bulk electron current. After the photocurrent is switched off the sheath begins to expand back since its length is too short to allow the replacement of the ions lost at the cathode by the avalanche initiated by the secondary emission electrons. The sheath field has recovered its initial shape between 10 and 100 μs. Figure 10(c) shows the time evolution of the ion current density on the cathode over 100 μs, and confirms that the relaxation of the sheath seems to be complete after this time. The charged particle density in the plasma takes a longer time to recover its initial value. The time variations of the current densities which are presented in Fig. 10 show that the total current is slightly smaller in case 2 (corresponding to the larger steady-state dc current) than in case 1. The small oscillations of the total current are probably due to the numerical method. However, the main features of the calculated current correspond to real physical phenomena: The first decrease of the total current immediately after the onset of the photoemission

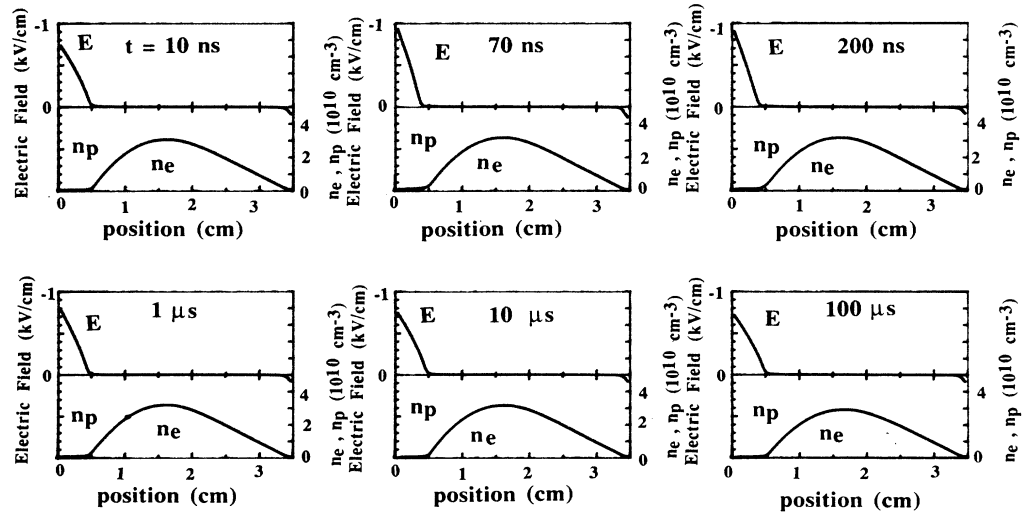

FIG. 9. Same as Fig. 8. Discharge conditions corresponding roughly to Fig. 6 (55 μA/cm^2, 224 V, but pure Ar, 0.25 Torr at 300 K).

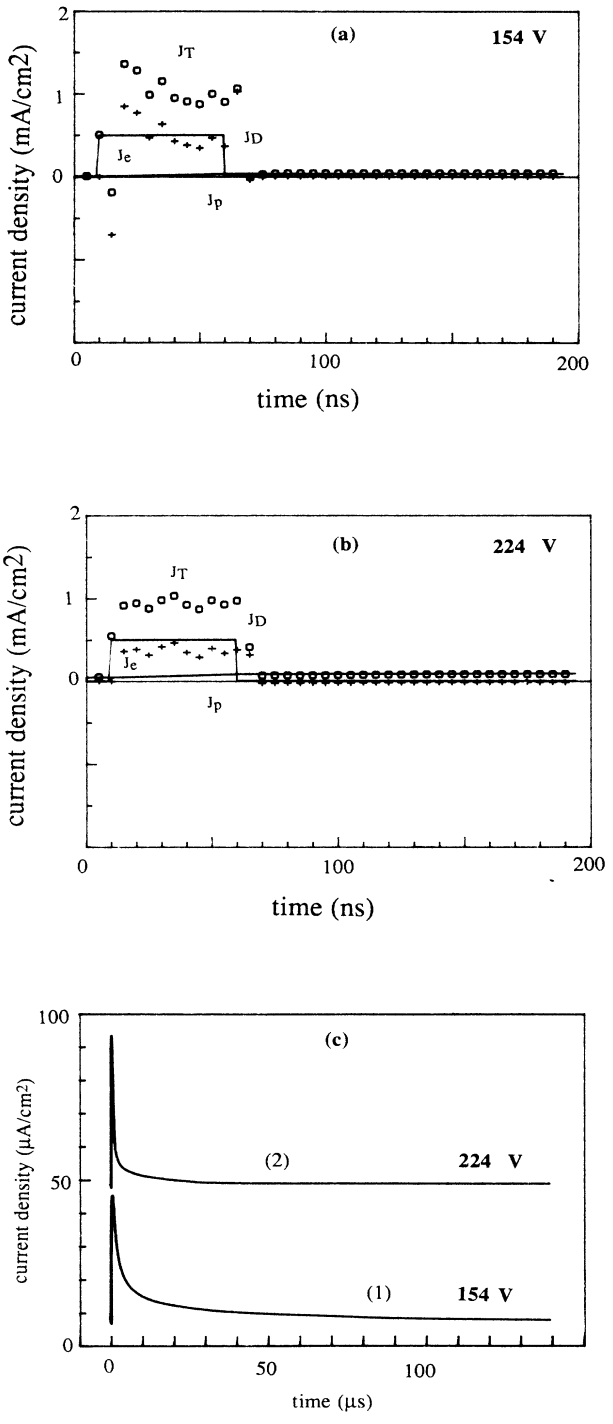

FIG. 10. (a) 8 μA/cm^2, 154 V, (b) 55 μA/cm^2, 224 V. Photoemission optogalvanic signal predicted by the numerical self-consistent macroscopic model (cf. Figs. 8 and 9). The total current density (○) as well as the displacement current density (+), electron and ion current densities (solid lines) on the cathode are presented. Some of the oscillations of the displacement current density are numerical. (c) Time evolution of the *ion* current density on the cathode for the conditions of (a) (1) and (b) (2) over 140 μs. To obtain the total current, one should add the electronic current plus the displacement current.

current in case 1 [Fig. 10(a)] is due to the instantaneous (the rise time of the pulse is supposed to be zero) injection of photoelectrons which leads to a sudden change in the space charge near the cathode and a decrease in the displacement current on the cathode. This effect does not appear in case 2 since the perturbation is relatively less important in that case (the photoemission current is about 60 times the steady-state unperturbed dc current in case 1, and 8 times the dc current in case 2). Note that for a photoemission current of 500 μA/cm^2 or larger, and assuming that the energy of the electrons leaving the cathode is of the order of one to a few eV, the space charge of these photoelectrons is not negligible with respect to the ion space charge in the sheath in case 1. The displacement current then increases due to the increase in the ion density in the sheath induced by the avalanching photoelectrons. When the photoemission current is switched off, the displacement current first increases on the cathode [Fig. 10(a)] due to the decrease in the electron space charge. The displacement current then decreases and changes its sign: There remains only the contribution of the (enhanced) ionic current plus a small negative displacement current (the magnitude of the sheath on the cathode starts to decrease). Note that due to our assumption that the beam releases its energy instantaneously in the discharge (the beam equations are steady-state equations in our model–see Sec. IV A) some of the above results concerning the time evolution of the current on the short-time scale (less than 10 ns) are questionable. However, we believe that the main features predicted by the model are realistic.

Most of these results are in excellent qualitative agreement with our experimental observations. Knowing the complexity and intricacy of the physical phenomena involved, this agreement is remarkable. The comparison of the absolute values of the calculated and measured total current seems to indicate that the photoemission current has been underestimated in the calculations.

On the other hand, we have performed numerical calculations in the case of a repetitive photoemission pulse (the repetition period was 150 μs, as in the experiment). The model predicts that the plasma density has not completely recovered its initial steady-state dc value after 150 μs, and continues to increase sligthly after each laser pulse (we obtain a 10% increase of the plasma density after 4 pulses for case 1). For a larger photoemission current (which seems to be the case in the experiment), this effect would be enchanced. Other kinds of plasma diagnostics probing ions[29–31] or electrons[32] would be needed to confirm experimentally this increase in the mean plasma density due to the repetition of the laser pulse.

Let us now try to estimate the validity of our self-consistent model. There are at least two assumptions in the model which are doubtful and could be responsible for some discrepancies between experimental and numerical results, and which should be checked before a quantitative description of the phenomena can be expected. (1) We have neglected the 2% K atoms. (2) The beam models ignore the fact that the electrons emitted by the cathode and accelerated in the sheath may be scattered in a direction other than forward. This indicates that the

ionization process may not be properly described in our model. To test this, we have performed complementary Monte Carlo simulations of the electron kinetics in the sheath.

D. Monte Carlo simulations of the ionization in the cathode region

Using the approach of Boeuf and Marode,[33] we assume in this simulation a given shape of the electric field and follow the trajectories of a large number of electrons emitted by the cathode. This method is therefore not self-consistent, but in contrast to the beam model, takes into account properly the scattering during electron-neutral collisions. We used this method to obtain the ionization rates in the actual experimental mixture 98% Ar, 2% K.

The numerical method is described in Ref. 33. The electron-atom cross sections in potassium vapor are taken from the work of Lucas.[34] The calculations provide the normalized ionization rates $\beta(x)$ in the discharge; the total ionization rate $\beta_T(x)$ is defined as follows:

$$\beta_T(x)=\alpha_T(x)\phi(x)/\phi(0)$$
$$=\alpha_T(x)\exp\left[\int_0^x \alpha_T(y)dy\right],$$

where $\alpha_T(x)$ is the local total ionization coefficient and $\phi(x)$ is the electron flux. Note that $M(x)=\phi(x)/\phi(0)$ is the electron multiplication at the position x, and that the area under the curve $\beta(x)$ is equal to the total multiplication plus one. It is also possible to define the partial ionization rates for the production of argon and potassium ions, respectively,

$$\beta_{Ar}(x)=\alpha_{Ar}(x)\exp\left[\int_0^x \alpha_T(y)dy\right],$$
$$\beta_K(x)=\alpha_K(x)\exp\left[\int_0^x \alpha_T(y)dy\right],$$

$\alpha_T=\alpha_{Ar}+\alpha_K$; α_{Ar} and α_K are the partial ionization coefficients for production of argon and potassium ions, respectively. These rates are plotted on Figs. 11 and 12 for cases 1 and 2, respectively. Figure 11 shows that the production of K^+ ions, if not negligible, remains, however, small compared with the production of Ar^+.

More interesting are the results shown in Fig. 12 where we compare the electron multiplication coefficient $M(x)$ (the "gain" of the avalanche) derived from the Monte Carlo simulation with the values underlying the self-consistent beam model. Although the relative difference in the magnitudes of the total gain $M(d)$ is 30%, of more concern to us is the difference in the shape of the curves. We see that the beam model, in contrast to the more exact prediction of the Monte Carlo simulation, yields to a large production of ions well beyond the sheath edge. This is especially striking in the case 2 (55 $\mu A/cm^2$, 224 V). Consequently, we may infer that the beam model simulation of the photoemission initiated avalanche tends to (a) overestimate the increase in the charge density in the bulk plasma, and (b) underestimate the perturbation of the cathodic field and therefore the total current, this underestimation being more severe in case 2 than in case 1.

This may explain, in particular, why case 2 is not so well reproduced as case 1 by the model. This also emphasized the need for models more realistic with respect to the ionization processes than the beam model. Similar conclusions have been drawn previously.[3,21] Note that the predictions of the beam model are not unphysical but tend to overestimate the penetration depth of the high-energy electrons in the glow; this penetration depth is not very large in our condition because the discharge regimes corresponding to cases 1 and 2 are not far from the normal regime. The Monte Carlo model as well as the beam models predict an increase in this penetration depth when the applied potential is increased.

Although, as we mentioned above, it seems rather difficult to develop a self-consistent fully microscopic (based on the solution of Boltzmann transport equations for electrons and ions, coupled with Poisson's equation) model, an easier way to improve our macroscopic model would be to use the same moment equations to describe the charged particle transport, but with a source term of the continuity equations (ionization) deduced from Monte Carlo simulations. This hybrid method (coupling

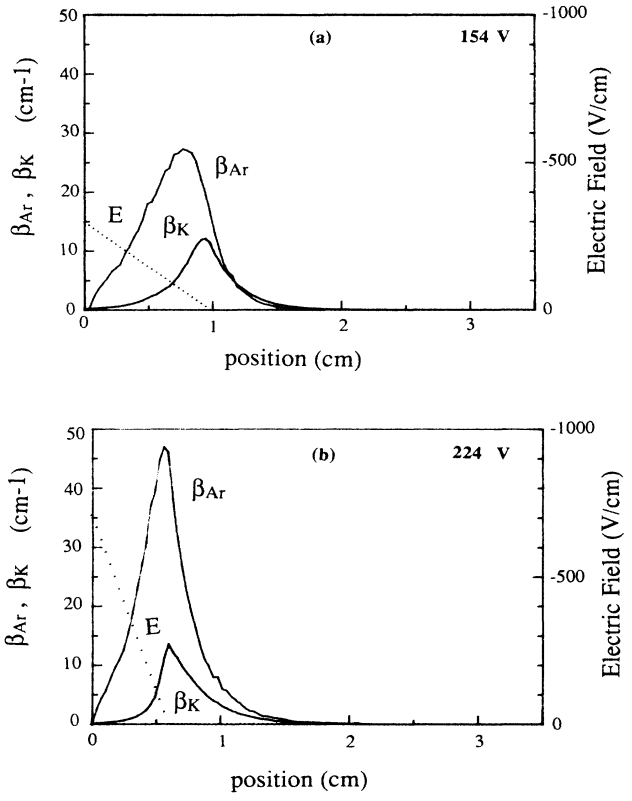

FIG. 11. Ionization in the sheath predicted by a Monte Carlo simulation assuming a linear decrease of the electric field in the sheath in the mixture Ar(98%)+K(2%) (0.25 Torr, 300 K). The electric field distribution is also plotted; the sheath length is deduced from the experiment: (a) 154 V, dc=10 mm, (b) 224 V, dc=6 mm.

of a macroscopic model of the particle transport with a microscopic estimation of the ionization term) can lead to a more accurate description of the discharge characteristics. This hybrid method has been used to obtain the self-consistent result presented in Fig. 13 (steady-state discharge corresponding to the unperturbed case 1; 98% Ar, 2% K mixture). The procedure used to obtain this result was as follows.

(a) For a given experimental field distribution, the ionization source terms (production of argon and potassium ions) are calculated with a Monte Carlo simulation.

(b) The calculated source terms are used in the macroscopic model to determine the self-consistent electric field and charged particle densities. The secondary-electron emission is adjusted so that the calculated field profile is similar to the experimental one.

Note (Fig. 13) that the density of potassium ions in the sheath is much smaller than the argon-ion density. This confirms the fact that the presence of potassium in the discharge would not change qualitatively (and not very much quantitatively) the results presented in Sec. IV C (where the concentration of potassium atoms had been neglected).

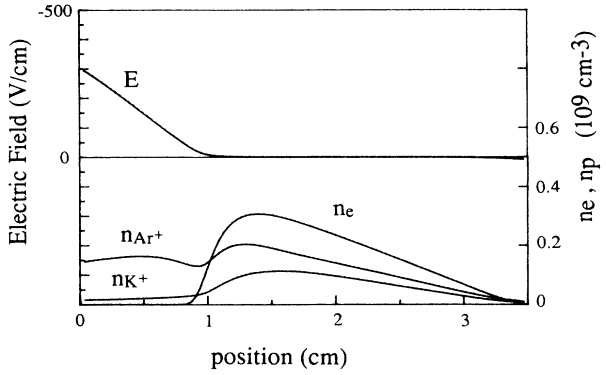

FIG. 13. Spatial variations of the electric field and charged particle distributions in the gap obtained in the Ar-K mixture for case 1 using a self-consistent macroscopic model where the ionization rates for the production of argon and potassium ions are deduced from a Monte Carlo simulation (hybrid model). The secondary-emission coefficient γ is adjusted so that the calculated field matches the experimental field; this led to $\gamma = 0.05$.

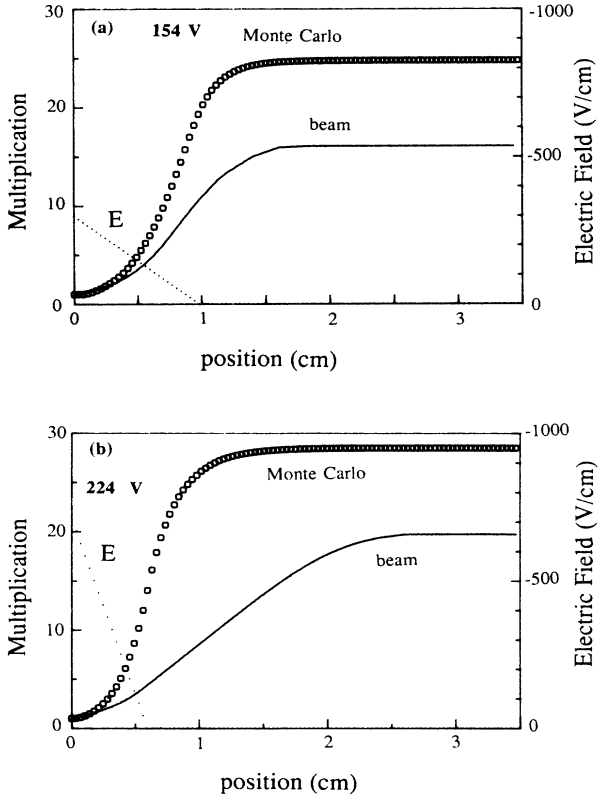

FIG. 12. Spatial variations of the total multiplication in the discharge calculated using a Monte Carlo simulation in Ar(98%)+K(2%) mixture (points); the electric field is also represented. Also shown for comparison are the multiplications deduced from the self-consistent beam model in pure argon (solid lines). Same conditions as Fig. 11: (a) 154 V, dc=10 mm, (b) 224 V, dc=6 mm. Note that the Monte Carlo simulation predicts that most of the ionization occurs in the sheath, contrary to the beam model.

Some more remarks should also be made about the dependence of the total electron multiplication coefficient $M(d)$ and the amplitude of the POG signal with discharge conditions. Mitchell *et al.*[3] observed that the POG signal amplitude strongly decreases with the discharge power. They attributed this decreasing to the fact that the sheath thickness decreases with the discharge power and claimed that so does the electron multiplication coefficient $M(d)$. But we did not observe such a power dependence (see Fig. 2) although our sheath thickness changes by 50% between cases 1 and 2. Indeed, Fig. 12 shows that $M(d)$ in cases 1 and 2 differ by only 15% (the larger M for the larger discharge power). We must, however, emphasize that our applied voltages correspond to the low-power regime of Mitchell *et al.*,[3] where they observe little power dependence. This just points out the fact that sheath thickness *and* voltage may be equally important in determining in the general case (especially close to the low-power or normal regime) the magnitude of $M(d)$ and thus the POG intensity.

V. CONCLUSION

In this work we have directly observed the motion of the sheath of a glow discharge subjected to a strong perturbation and the subsequent relaxation back to steady state. It has been demonstrated that the coupling of sophisticated optical diagnostic techniques and numerical models can yield insight into the discharge mechanisms and can be used to characterize dc as well as transient (for example rf) discharges.

Most of the physical processes involved seem to be understood. The comparison of the experimental results with the predictions of a self-consistent macroscopic model where cathode emitted electrons are supposed to

form a monoenergetic beam is good and shows the ability of such a model to reproduce the observed phenomena in a detailed way. From a quantitative point of view, the beam model is, however, adequate only in a limited range of discharge conditions, and a better estimation of the ionization rates by fast electrons in the cathode region can be obtained from Monte Carlo simulations. In the general case sheath thickness and voltage are equally important in determining the amplitude of the optogalvanic signal which results from the photoelectron avalanche.

There are other points which deserve further investigation. They include the following: optical diagnostics of ions[29–31] and electron[32] distributions; optical diagnostics at a very short-time scale (~ 10 ns) to directly probe the electron avalanching; optical diagnostics spatially resolved in the radial direction to probe the two-dimensional aspect of the phenomena; study of the influence of the photoemission pulse duration, and of the time interval between photoemission pulses and POG signals; and study of the influence of a variation of the applied voltage during the electron avalanche and/or the relaxation with relevance to application to rf discharge diagnostics.

ACKNOWLEDGMENTS

We gratefully acknowledge M. P. Alberta for her very valuable help in taking the data. It is a pleasure to acknowledge R. A. Gottscho for communicating results prior to publication and for numerous suggestions and comments in the preparation of this paper. We thank also J. Jolly who helped in transferring data between computers. This work was supported by DRET, Contract No. 88-108, and by GRECO 57. Laboratoire de Spectrométrie Physique is Unité associé au Centre National de la Recherche Scientifique No. 08. Centre de Physique Atomique de Toulouse is Unité associé au Centre National de la Recherche Scientifique No. 277.

[1]S. W. Downey, A. Mitchell, and R. A. Gottscho, J. Appl. Phys. **63**, 5280 (1988).

[2]G. S. Selwyn, B. D. Ai, and J. Singh, Appl. Phys. Lett. **52**, 1953 (1988).

[3]A. Mitchell, G. R. Scheller, R. A. Gottscho, and D. B. Graves, preceding paper, Phys. Rev. A **40**, 5199 (1989).

[4]R. N. Varney, Phys. Rev. **93**, 1156 (1954).

[5]C. A. Moore, G. P. Davis, and R. A. Gottscho, Phys. Rev. Lett. **52**, 538 (1984).

[6]R. A. Gottscho, Phys. Rev. A **36**, 2233 (1987).

[7]J. Derouard and M. H. Alexander, J. Chem. Phys. **85**, 134 (1986).

[8]J. Derouard and N. Sadeghi, Opt. Commun. **57**, 239 (1986).

[9]J. Derouard, H. Debontride, and N. Sadeghi, J. Phys. (Paris) Colloq. **48**, C7-725 (1987).

[10]J. Derouard, H. Debontride, T. D. Nguyen, and N. Sadeghi, J. Chem. Phys. **90**, 5936 (1989).

[11]Stainless steel is mostly composed of Fe, Ni, and Cr, whose electron work functions are 4.5, 5.1, and 4.5 eV, respectively (see Ref. 12).

[12]*CRC Handbook of Physics and Chemistry,* 68th ed., edited by R. C. Weast and M. J. Astle (CRC Press, Boca Raton, FL, 1987).

[13]R. E. Drullinger and R. N. Zare, J. Chem. Phys. **51**, 5532 (1969); **59**, 4255 (1973).

[14]G. Francis, *The Glow Discharge at Low Pressure,* Vol. 22 of *Handbuch der Physik,* edited by H. S. Flugge (Springer, Berlin, 1956), p. 53.

[15]A. Von Engel, *Ionized Gases* (Clarendon, Oxford, England, 1965).

[16]R. Warren, Phys. Rev. **98**, 1650 (1955).

[17]S. A. Lee, L. U. A. Andersen, J. J. Rocca, M. Marconi, and N. D. Reesor, Appl. Phys. Lett. **51**, 409 (1987).

[18]A. V. Phelps, B. M. Jelenkovic, and L. C. Pitchford, Phys. Rev. A **36**, 5237 (1987).

[19]J. P. Boeuf, Phys. Rev. A **36**, 2782 (1987).

[20]J. P. Boeuf and P. S. Ségur, in *Interactions Plasma Froids Materiaux,* GRECO 57 CNRS, edited by C. Lejeune (Les Editions de Physique, Paris 1988), p. 113.

[21]R. A. Gottscho, A. Mitchell, G. R. Scheller, N. L. Schryer, D. B. Graves, and J. P. Boeuf, in *Proceedings of the Seventh Symposium Plasma Processing Electrochemical Society,* edited by G. S. Mathad, G. C. Schwartz, and D. W. Hess (Electrochem. Soc., Pennington, NJ, 1988).

[22]M. Kurata, *Numerical Analysis for Semiconductor Devices* (Heath, Lexington, MA, 1982).

[23]A. L. Ward, J. Appl. Phys. **33**, 2789 (1962).

[24]J. Bretagne, G. Callede, M. Legentil, and V. Puech, J. Phys. D **19**, 761 (1986).

[25]B. Chapman, *Glow Discharge Processes* (Wiley, New York, 1980).

[26]D. B. Graves and K. F. Jensen, IEEE Trans. Plasma Sci. **PS-14**, 78 (1986).

[27]R. A. Gottscho, A. Mitchell, G. R. Scheller, Y. Y. Chan, and D. B. Graves, Phys. Rev. A (to be published).

[28]J. P. Boeuf, J. Appl. Phys. **63**, 1342 (1988).

[29]R. Walkup, R. W. Dreyfus, and P. Avouris, Phys. Rev. Lett. **50**, 1846 (1983).

[30]R. A. Gottscho, R. H. Burton, D. L. Flamm, V. M. Donnelly, and G. P. Davis, J. Appl. Phys. **55**, 2707 (1983).

[31]A. Margulis and J. Jolly, Rev. Phys. Appl. **24**, 323 (1989).

[32]E. A. Den Hartog, T. R. O'Brian, and J. E. Lawler, Phys. Rev. Lett. **62**, 1500 (1989).

[33]J. P. Boeuf and E. Marode, J. Phys. D **15**, 2169 (1982).

[34]J. Lucas, in *Electron and Ion Swarms,* Proceedings of the Second International Swarm Seminar, edited by L. Christophorou (Pergamon, New York, 1981), Vol. 231; S. A. J. Al Amin and J. Lucas, J. Phys. D **21**, 1261 (1988).